



A computational investigation of unsteady turbulent wake–boundary-layer interaction

Z. Gete, R.L. Evans*

Department of Mechanical Engineering, The University of British Columbia, 2324 Main Mall, Vancouver, BC, Canada V6T 1Z4

Received 12 May 2001; accepted 16 April 2003

Abstract

The relative motion of rotor and stator blade rows in a turbomachine generates periodically unsteady flow on the blades due to travelling wake perturbations. To better understand the attendant wake–boundary-layer interaction a calculation procedure was developed to model the behaviour of this complex unsteady flow. Due to nonlinear interactions with the boundary layer, the travelling discrete frequency wakes were found to decrease the velocity profile shape factor. For the range of reduced frequencies examined ($\varpi = 0.33–9.33$) the skin-friction coefficient was found to be frequency dependent. The calculated results for both steady and unsteady velocity profiles, and for skin friction compared well with experimental data. Although the agreement between measured and calculated velocity phase shift was poor, in both experimental and model results the negative phase shift throughout the boundary layer due to the travelling-wave fluctuations has been captured.

© 2003 Elsevier Ltd. All rights reserved.

1. Introduction

Turbulent boundary layers on turbomachinery blading are three-dimensional and highly unsteady. Various factors contribute to the generation of unsteadiness in turbomachinery flow. Among those factors are the free-stream turbulence, periodic wakes shed and transported from upstream blades, upstream potential interaction due to the relative motion of blades, inlet flow distortions, rotating stall, end wall effects, leakage, wall roughness, etc. It is difficult if not impossible to determine the relative importance and contributions of all factors simultaneously.

The unsteady interactions of the rotating and stationary blade rows in an axial flow turbomachine affect many aspects of performance such as blade loading, stage efficiency, heat transfer, stall margin and noise generation, as noted by Hodson (1984a, b). The aerodynamic loading of a blade in a real machine varies with a change in incidence angle of the oncoming flow and the relative velocity associated with it. The relative velocity at the exit of an upstream rotor or stator exhibits a velocity deficit in the wake region, and therefore a downstream blade exposed to such fluctuations is subject to variations in aerodynamic loading. The velocity defect, or wake, moves downstream as a travelling-wave-type disturbance with a finite speed Q and intermittently perturbs the boundary layer on a downstream blade with a discrete frequency. This interaction strongly influences the development of the boundary layers and it is therefore necessary to estimate the effect of the unsteadiness on losses, skin friction and flow development inside the blade passages.

An experiment that focused on unsteady wake–boundary-layer interaction has been conducted previously on a two-dimensional rotor–stator model in a wind tunnel, schematically shown in Fig. 1. Moving airfoils represented the rotor and a flat plate was used to represent a stator blade. Experimental data from the wake–boundary-layer interaction measurements were used for comparison with the computational scheme described in this paper.

*Corresponding author.

E-mail address: evans@mech.ubc.ca (R.L. Evans).

Nomenclature

A	constant
b	constant $(1 + \varepsilon_m^+)$
C	absolute velocity (m/s)
C_f	skin-friction coefficient
$(C_f)_{\text{avg}}$	average skin-friction coefficient
f	dimensionless stream function, wake generation frequency (Hz)
f'	dimensionless velocity $(u/U_0), u(x, \eta, t)$
f''	wall friction parameter $(u/U_0)'$
P	dimensionless pressure $((x/U_0) dU_e/dx)$
P_3	dimensionless free-stream pressure: $(x/U_0^2)(U_e \partial U_e/\partial x + \partial U_e/\partial t)$
Q	travelling wave velocity (m/s)
Re_x, Re	Reynolds number $U_e X/\nu$
R_θ	Reynolds number based on momentum thickness
S	airfoil spacing (m)
T	period
t	time coordinate, time (s)
t_0	initial time (s)
U_0, U_∞	average free-stream velocity (m/s)
U_e	fluctuating free-stream velocity (m/s)
ΔU_e	amplitude of fluctuating free-stream velocity
U_r	rotor or blade velocity (m/s)
$u\tau$	friction velocity $\sqrt{\tau_w/\rho}$
u	velocity in the longitudinal direction (m/s)
v	velocity in the transverse direction (m/s)
$V(x, \eta, t)$	a variable defined as $u'(x, \eta, t)$
X, x	horizontal coordinate axis, longitudinal position (m)
y	transverse position (m) or transverse axis
α	a coefficient in the eddy viscosity model for the outer region given as a function of R_θ
ε_m	eddy viscosity
$(\varepsilon_m)_I$	eddy viscosity in the internal region of the boundary layer
$(\varepsilon_m)_0$	eddy viscosity in the outer region of the boundary layer
$(\varepsilon_m)^+$	dimensionless eddy viscosity ε_m/ν
η	dimensionless transverse coordinate $y(\sqrt{U_0/\nu x})$
η_∞	transverse position at free stream
$\Delta\eta$	grid spacing in the transverse direction
ν	kinematic viscosity (m^2/s)
ρ	fluid density (kg/m^3)
τ	boundary-layer shear stress
τ_w	wall shear stress
ψ	stream function
ω	fluctuation frequency (rad/s)
ϖ	reduced frequency fX/U_0

2. Computational scheme

Since the governing equations for flows of practical interest are often complicated, an exact solution is not usually available. Instead, approximate solutions are developed using computational fluid dynamic (CFD) techniques. CFD complements experimental and theoretical fluid dynamics by providing a cheaper and faster alternative for modelling real flows. In this process appropriate discretization of the governing equations must be performed prior to carrying out the computation. The required number of grid points for accurate solution depends on the geometric complexity and

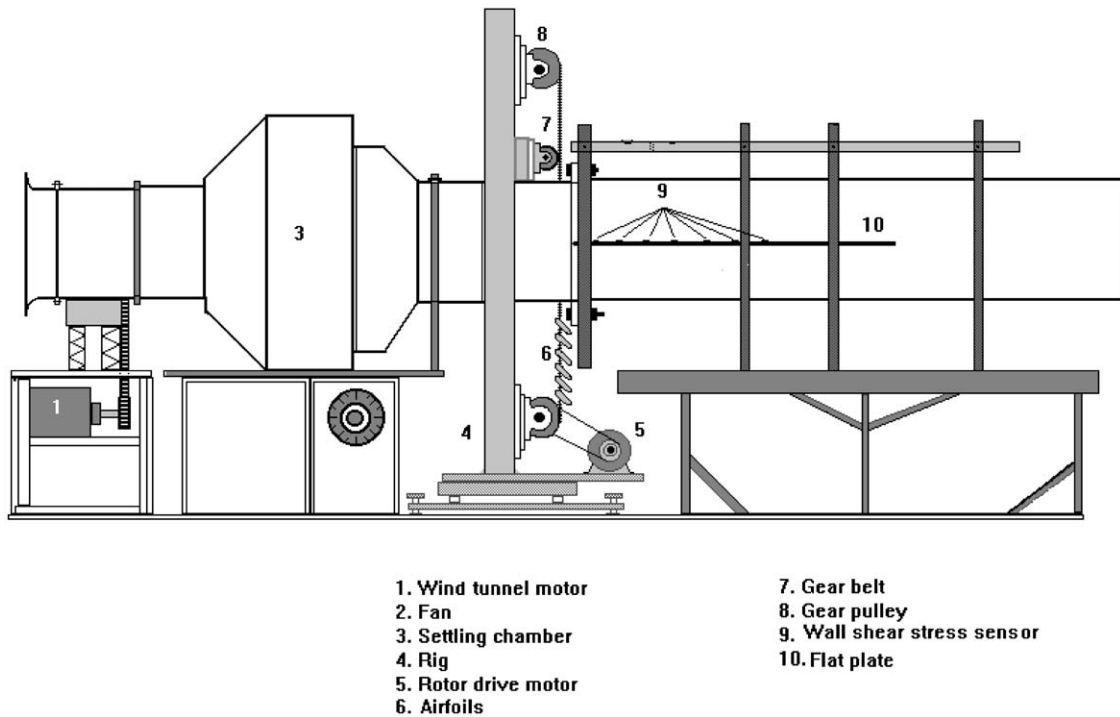


Fig. 1. Wind tunnel and experimental set-up.

severity of the gradients of the dependent variables. In addition, due to the nonlinearity of the governing equations, the computational solution usually proceeds iteratively.

Despite the widespread existence of travelling-wave free-stream disturbances in fluid machinery, the nature of this type of wake–boundary-layer interaction and its impact on the wall shear stress, phase shifts, etc., are not clearly understood. In this paper, a computational scheme for predicting the behaviour of a turbulent boundary layer subjected to a sinusoidal travelling-wave-type external disturbance is presented. Calculations of turbulent boundary-layer development on a flat plate under the influence of a periodic free-stream velocity have been performed, and compared to experimental data.

The numerical procedure of [Cebeci and Carr \(1978\)](#) was modified to accommodate travelling-wave-type disturbances. [Evans \(1989\)](#) first modified this code to accommodate both standing and travelling-wave free-stream conditions for laminar boundary layers, while [Fletcher et al. \(1987\)](#) also used a similar procedure to solve turbulent boundary layers under the influence of standing-wave free-stream fluctuations.

Laminar boundary-layer computations by [Evans \(1989\)](#) for a standing-wave free-stream disturbance showed close agreement with the experimental data obtained from the work of [Lighthill \(1954\)](#), [Hill and Stenning \(1960\)](#), and [Patel \(1975\)](#). The calculations provided a perspective on the response of the boundary layer when subjected to these types of fluctuations, and also highlighted the important differences in boundary-layer response when subjected to disturbances of the travelling-wave type as compared to standing-wave perturbations. For example, the phase shift, which is a measure of the time it takes (with respect to the free-stream condition) for the boundary layer to respond to an external fluctuation, may show the velocity within the boundary layer to either lead or lag the externally imposed fluctuation, depending on the nature of the external disturbance. [Evans's \(1989\)](#) results showed that standing-wave-type external disturbances exhibit a phase lead, while travelling-wave-type disturbances result in a phase lag of the velocity within the boundary layer compared to the free-stream velocity.

Studies conducted by [Carr \(1981\)](#) on unsteady turbulent boundary layers perturbed by standing waves demonstrate that the time-averaged mean velocity is nearly invariant over a range of frequencies, even for high amplitude fluctuations in the free-stream flow. In this case the time mean velocity profile of the boundary layer remains unchanged, and appears as one would expect for a steady flow with the mean velocity of the oscillating outer flow.

The purpose of developing the computational scheme in this study was not to present stand-alone results for unsteady turbulent boundary layers, but to provide a comparison with experimental results obtained by [Gete \(1996\)](#), as reported

by Gete and Evans (2003). The free-stream amplitude, frequency, and travelling-wave velocity obtained during the experiments were then used as inputs to the calculations. There is an implied assumption in using these experimental data in the computational scheme that the free-stream periodic fluctuations are sinusoidal. The assumption of sinusoidal free-stream conditions is a likely source of error when the results obtained by computation are compared to the experimental data.

2.1. Equations of motion

For a two-dimensional, incompressible, unsteady turbulent boundary layer, the governing differential equations are expressed as

$$\frac{\partial u}{\partial x} + \frac{\partial v}{\partial y} = 0, \quad (1)$$

$$\frac{\partial u}{\partial t} + u \frac{\partial u}{\partial x} + v \frac{\partial u}{\partial y} = \frac{\partial U_e}{\partial t} + U_e \frac{\partial U_e}{\partial x} + \frac{\partial}{\partial y} \left((v + \varepsilon_m) \frac{\partial u}{\partial y} \right). \quad (2)$$

These equations cannot be solved without additional closure equations for the turbulence stress terms. With a turbulence model of the eddy viscosity type and the pertinent boundary conditions, the governing equations can then be solved numerically. Two separate algebraic equations are formulated for the eddy viscosity. One of the equations treats the inner part of the profile while the other equation expresses the eddy viscosity in the outer region of the boundary layer.

For the inner region, the eddy viscosity equation reads

$$(\varepsilon_m)_i = \{0.4y[1 - \exp(-y/A)]\}^2 \left| \frac{du}{dy} \right|. \quad (3)$$

For the outer region, the eddy viscosity is modelled as

$$(\varepsilon_m)_0 = \alpha \int_0^\infty (U_e - u) dy. \quad (4)$$

In the above equations, A and α are given in the following forms:

$$A = 26v \frac{1}{u_\tau} \left\{ 1 - 11.8 \left[\frac{v}{U_e^3} \frac{\partial U_e}{\partial t} + \frac{U_e v}{u_\tau} \frac{dU_e}{dx} \right] \right\}^2,$$

$$\alpha = 0.0168 \frac{1.55}{1 + \left\{ 0.55 \left[1 - \exp \left(-0.243 \sqrt{\frac{R_\theta}{425} - 1} - 0.298 \left(\frac{R_\theta}{425} - 1 \right) \right) \right] \right\}}.$$

The boundary-layer equations, and the boundary conditions are expressed in terms of transformed variables

$$x = x, \quad t = t, \quad \eta = y(U_0/\nu x)^{1/2}.$$

Defining a dimensionless stream function $f(x, t, \eta) = \psi / \sqrt{\nu x U_0}$, the transformed governing equation and the boundary conditions become

$$(bf'')' + \frac{P+1}{2} ff'' - P(f')^2 + P_3 = x \left(f \frac{\partial f'}{\partial x} - f'' \frac{\partial f}{\partial x} + \frac{1}{U_0} \frac{\partial f'}{\partial t} \right), \quad (5)$$

where

$$f' = \frac{u}{U_0}, \quad P = \frac{x}{U_0} \frac{dU_e}{dx}, \quad P_3 = \frac{x}{U_0^2} \left(U_e \frac{\partial U_e}{\partial x} + \frac{\partial U_e}{\partial t} \right),$$

$$b = 1 + \varepsilon_m^+, \quad \varepsilon_m^+ = \frac{\varepsilon_m}{\nu}$$

and the boundary conditions transform to

$$\text{at } \eta = 0, \quad f = f' = 0,$$

$$\eta \rightarrow \eta_\infty, \quad f' = \frac{U_e}{U_0}.$$

By introducing new dependent variables $u(x, \eta, t)$ and $V(x, \eta, t)$ to Eq. (5), where $f' = u$ and $u' = V$ the algebraic equations in the flow domain can be solved. For further details of the computational formulations, reference should be made to the paper by Cebeci and Carr (1978).

2.2. Numerical formulation

A numerical scheme for predicting unsteady travelling-wave-type turbulent boundary layers was developed by modifying the unsteady laminar scheme of Evans (1989), and was used to predict the experimental flow described by Gete and Evans (2003). All calculations are based on the finite-difference method developed by Cebeci and Smith (1974) and later modified by Evans (1988) to accommodate travelling-wave free-stream disturbances. The numerical formulation chosen was the Keller “box” method, as reported by Cebeci and Bradshaw (1977). One advantage of the Keller box method is that nonuniform grid spacing can be used both across the boundary layer, in the streamwise direction, and in the time dimension. This method uses the basic idea of writing the governing system of equations in the form of a first-order system. The resulting first-order equations are formulated by centred-difference derivatives and averages at the midpoints of net rectangles and net segments formed by the discretization process. As a result, a system of implicit, nonlinear algebraic equations are generated throughout the calculation domain. For solution, Newton’s method was employed.

In applying this method to the wake–boundary-layer interaction in the flow domain, the free-stream velocity was represented by a travelling-wave-type sinusoidally fluctuating velocity expressed as

$$U_e(x, t) = U_0 + \Delta U_e \sin \omega(t - x/Q), \quad (6)$$

where U_0 is the time-averaged mean velocity, ΔU_e is the amplitude in the free stream and Q is the velocity of the travelling wave.

The procedure calls for the turbulent boundary layer on the flat plate to be discretized in time and in the longitudinal, and transverse dimensions. The period for any cycle was determined from the experiments and equal time steps were used during computation. The streamwise dimension had unequal grid spacing equivalent to the measurements ($X = 0.1, 0.2, 0.3, 0.4, 0.5, 0.6, 0.7$ m). The flow was specified to be turbulent starting from the location of the trip wire ($X = 0.02$ m). The grid spacing across the boundary layer was nonuniform and was generated by a geometric progression where the ratio of any two adjacent intervals is a constant.

At each downstream location, the solution marches in the time direction; then the governing equations are solved for each specified time station. The linearized forms of the equations were solved iteratively until a prescribed convergence criterion was met. The code uses the wall shear stress parameter $\{f_w'' = (u/U_0)'\}$ as the basis for convergence. Calculation terminated when $2\delta f_w''/\delta f_w'' + 2f_w'' < 0.1$. For turbulent boundary layers subjected to travelling-wave-type fluctuations, the solutions were sensitive to the time and transverse spacing. Therefore, the smallest time and vertical space scales that could be resolved were limited to the order of 1 ms and 0.02, respectively.

2.3. Boundary and initial conditions

The measured travelling speed of the disturbance for all experimental cases investigated was about 0.8 times the local free-stream velocity. The velocity in the boundary-layer approaches the external fluctuating velocity in the free stream at the outer edge, while all quantities with the exception of the wall shear stress vanish at the plate surface. With proper specification of initial conditions at some initial upstream surface the problem is then completely formulated. The conditions required in these case are

$$t = t_0 \quad \text{and} \quad x \geq x_0, \quad u = u_0(x, \eta);$$

$$x = x_0 \quad \text{and} \quad t \geq t_0, \quad u = u_0(\eta, t).$$

These conditions provide velocity distributions everywhere at some initial time, and for subsequent time, conditions are given on some upstream station. When the conditions are applied to Eq. (3), initial velocity fields can be obtained.

Table 1 shows the experimental conditions used in the computational scheme. The table shows values of the rotor linear velocity U_r , the spacing between airfoils S , the frequency of blade passage f and the rotational speed, ω , the period T and the amplitude ΔU_e of the free-stream fluctuations. These values were either conditions imposed during the experiments, or measured results obtained and used as inputs to the calculations.

Table 1

Experimental conditions and results applied to the computation: $U_\infty = 3.0$ m/s

Rotor velocity, U_r (m/s)	Rotor spacing, S (m)	Frequency, f (Hz)	Speed, ω (rad/s)	Period, T (s)	Amplitude, ΔU_e (%)
2.0	0.1	20	125.66	0.05	10
3.0	0.1	30	188.49	0.033	10
4.0	0.1	40	251.33	0.025	10

3. The experiment

Experimental data obtained in a wind tunnel was used for comparison with the results of the calculation scheme. A turbomachinery stage was represented with a two-dimensional rotating rig and a flat plate arrangement in a wind tunnel. Complete details have been reported by Gete and Evans (2003). The moving mechanism has airfoils (“rotor” blades) attached to rotating synchronized gear belts thereby generating travelling periodic wake disturbances in the oncoming air-flow. Fig. 1 shows the wind tunnel along with the unsteady flow-generating rig. The flat plate had a 0.8 mm diameter trip wire located 20 mm from the leading edge, and due to the spacing on the belt only a single row of blades passed in front of the flat plate at any one time. The ratio of the transverse “rotor” speed U_r to the blade spacing S determines the frequency f of the wake disturbances passing in front of the flat plate. Normalizing the frequency with the free-stream velocity U_∞ and the downstream length X generated a range of intermediate reduced frequencies, $\varpi = fX/U_\infty$ from 0.33 to 9.33. The undisturbed free-stream velocity, U_∞ , was set to 3.0 m/s for all experiments, and the transverse rotor velocity, U_r , ranged between 2.0 and 4.0 m/s.

The experimental study included measurement of the unsteady boundary-layer velocity profile and turbulence intensity using a hot wire probe, and measurement of the wall shear stress using glue-on shear stress probes. The resulting data were analysed to investigate the effect of disturbance frequency on velocity profile, velocity phase shift, and the wall shear stress. The experimental data were then used for comparison with the results of the calculation scheme.

4. Computational results and comparison with experiments

4.1. Boundary-layer velocity profiles

One of the outputs from the computation process was the velocity profile across the turbulent boundary layer. The calculations furnish values of the dimensionless velocity f' with respect to the similarity variable η or the coordinate y . Calculations were first conducted assuming steady flow, and compared to measurements on the flat plate without the “rotor” blade moving. Fig. 2 illustrates results of the steady turbulent boundary-layer profiles obtained at several longitudinal locations on the flat plate. Fig. 3 shows a comparison of calculated and experimental results of the steady velocity profiles. The results are in good agreement except at $X = 0.1$ m where the calculated values over predict the experimental values. The discrepancy at this station indicates that the experimental velocity profile was not yet fully turbulent.

The remaining figures show the results of unsteady calculations at various frequencies, and in all cases an amplitude of free-stream fluctuations equal to 10% of the mean free-stream velocity. Calculated phase-averaged unsteady turbulent boundary-layer velocity profiles for a frequency of the external fluctuations of 20 Hz are shown for various phase angles in Fig. 4. The outstanding feature of the profiles is the unsteadiness generated throughout the boundary layer due to the interactions of the oscillatory free-stream disturbance with the steady turbulent boundary layer. It is apparent that the velocity profiles vary significantly from phase to phase. The response of the boundary layer is more accentuated in the outer region than in the inner region. For instance, looking at the profiles at $X = 0.3$ m, the fluctuation amplitude reaches up to 20% of the mean velocity in the external region of the boundary layer. The profile fluctuations are, however, stronger in the internal region here than was the case in the experimental results. In general, the shape factor decreases as the velocity defect goes towards its maximum, then increases as the flow accelerates and the defect decreases. Some of the profiles appear to revert to transition-like behaviour during some of the phases in a cycle.

Figs. 5–7 compare calculated and measured averaged velocity profiles at the indicated frequencies. Although the calculated average velocity profiles underestimate the experimental results, particularly at downstream stations for $f = 20$ Hz, the agreement improves as the frequency is increased. Comparison of calculated and measured velocity

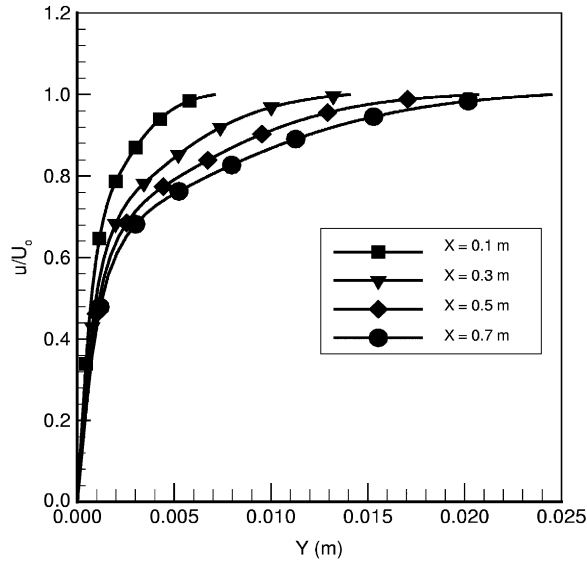


Fig. 2. Calculated turbulent boundary-layer velocity profiles along the flat plate in steady flow.

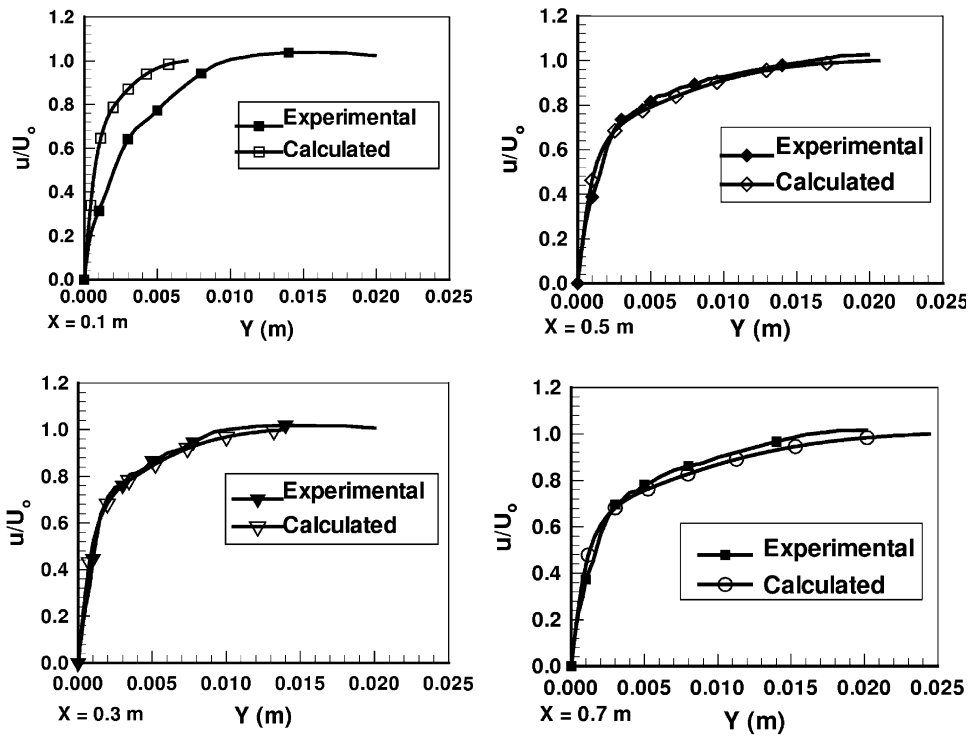


Fig. 3. Comparison of experimental and calculated steady turbulent boundary-layer velocity profiles: (a) $X = 0.1$ m, (b) $X = 0.3$ m, (c) $X = 0.5$ m, and (d) $X = 0.7$ m.

phase shifts is shown in Fig. 8. Both calculation and experiment show a similar qualitative trend although quantitative agreement is poor. Poor agreement is likely due in large part to the fact that the experimental free-stream fluctuations are not sinusoidal in nature.

As opposed to the interaction of standing-wave perturbations with the boundary layer, which generates a velocity phase advance (phase lead), travelling-wave-type interactions with the boundary layer impose a negative velocity phase

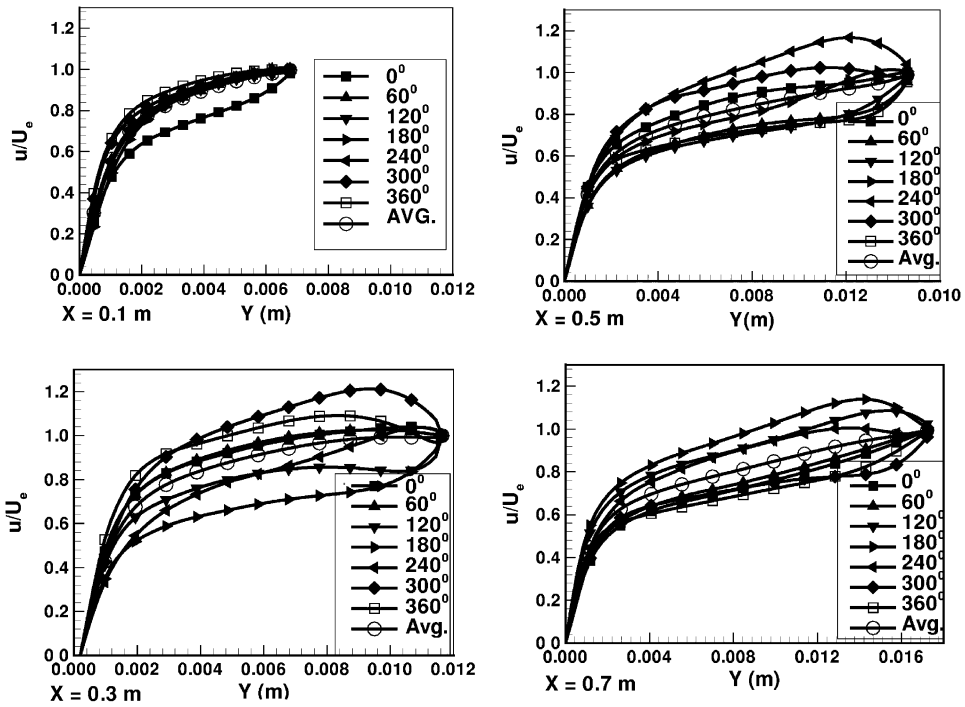


Fig. 4. Calculated phase-averaged velocity profiles under travelling-wave free-stream fluctuation at several downstream locations; $f = 20$ Hz: (a) $X = 0.1$ m, (b) $X = 0.3$ m, (c) $X = 0.5$ m, and (d) $X = 0.7$ m.

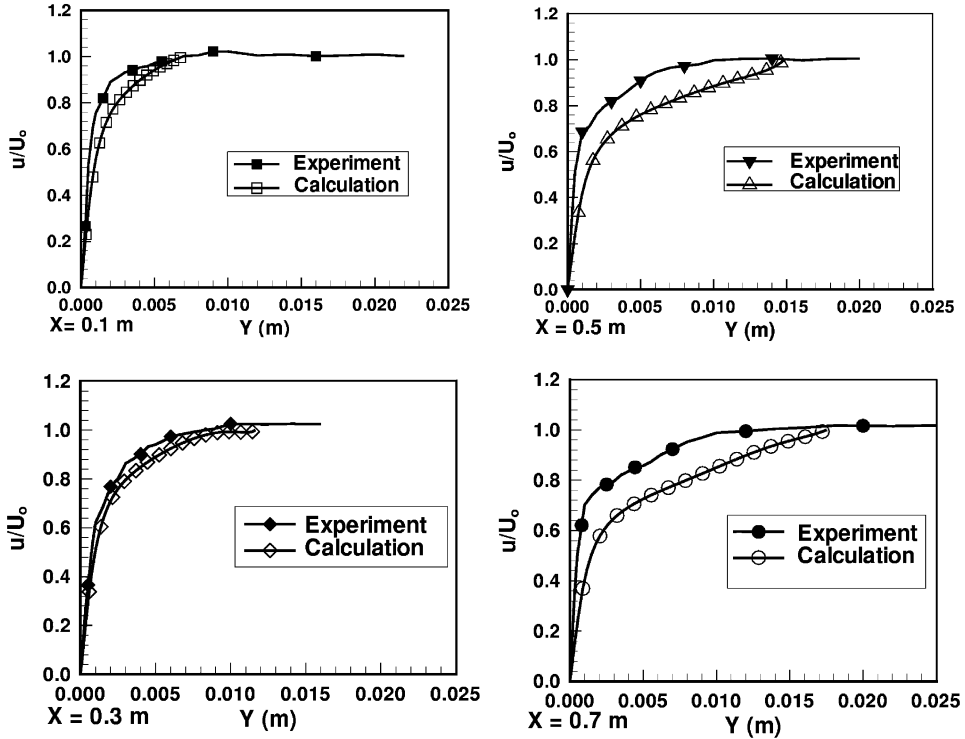


Fig. 5. Comparison of experimental and calculated average velocity profiles on the flat plate; $f = 20$ Hz: (a) $X = 0.1$ m, (b) $X = 0.3$ m, (c) $X = 0.5$ m, and (d) $X = 0.7$ m.

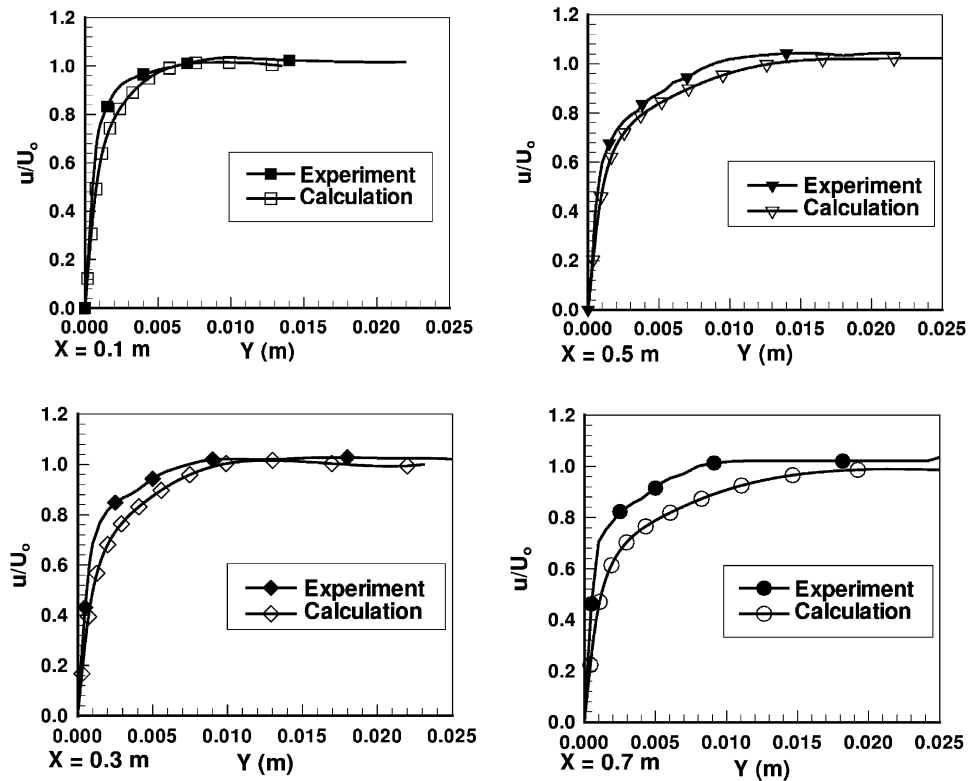


Fig. 6. Comparison of experimental and calculated average velocity profiles on the flat plate; $f = 30$ Hz: (a) $X = 0.1$ m, (b) $X = 0.3$ m, (c) $X = 0.5$ m, and (d) $X = 0.7$ m.

shift (phase lag) as indicated in the figure. The calculation procedure has successfully captured this important feature of travelling-wave-type unsteady boundary-layer behaviour.

4.2. Shear stress profiles

The calculation scheme provides shear stress values across the boundary layer. Although no measurement of shear stress was taken across the boundary layer (except at the wall) in any of the experiments, the computational results give some indication of what to expect due to the external disturbances. Fig. 9 shows the calculated shear stress results at various phases in a period for a frequency of 30 Hz. All cases show similar behaviour with strong shear stress fluctuations at the wall. The values of the shear stress reach maxima at or very close to the wall, and then decay at a fast rate to about the $\eta = 2.0$ location and remain almost flat for the remainder of the profile. It appears that the shear stress is less frequency sensitive in the outer region than in the inner region.

4.3. Skin-friction coefficient

Skin-friction calculations for unsteady turbulent boundary layers under travelling-wave disturbances are very scarce, although the state of wall shear stress under these circumstances is of enormous practical importance. Hence, the computational scheme was expanded to include prediction of skin friction in a turbulent boundary-layer subject to free-stream perturbations. As has been noted in the previous section, the code calculates the shear stress across the whole boundary layer at each η or y location. The skin-friction coefficient ($C_f = 2\tau_w/\rho U_\infty^2$) was therefore obtained from the shear stress at the surface of the flat plate. The wall shear stress was first computed for steady turbulent boundary-layer flows by setting the free-stream fluctuations to zero. Calculations of unsteady turbulent boundary-layer wall friction then followed, once the code was deemed to be valid for steady flows. The calculation domain covered stations from $X = 0.1$ to 0.7 m.

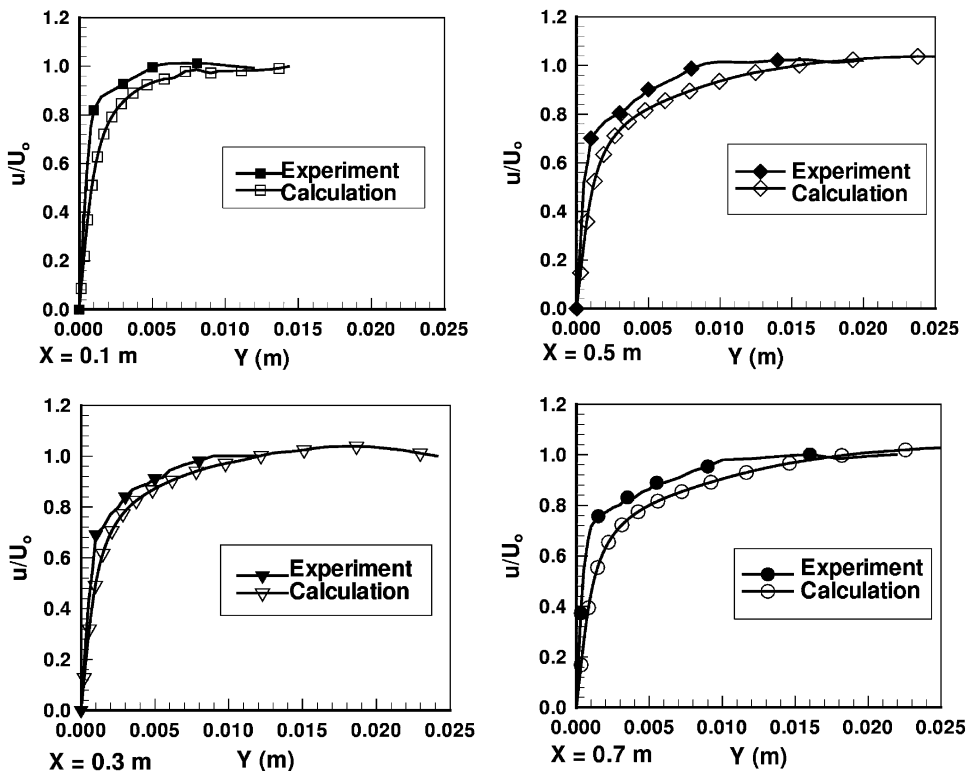


Fig. 7. Comparison of experimental and calculated average velocity profiles on the flat plate; $f = 40$ Hz: (a) $X = 0.1$ m, (b) $X = 0.3$ m, (c) $X = 0.5$ m, and (d) $X = 0.7$ m.

Fig. 10 shows calculated values of the average skin-friction coefficients in terms of the Reynolds number based on the longitudinal distance, X , for steady flow and for several frequencies. The unsteady skin-friction coefficient is seen to be considerably larger in all cases compared to that for the steady flow case. For instance, at a Reynolds number of 2×10^4 the skin-friction coefficient for a frequency of 40 Hz is twice the steady value. Variations are greatest near the leading edge, but appear to converge in the downstream direction. The results show the strong frequency dependence of the response of the unsteady wall shear stress to travelling free-stream fluctuations. Within the range of the frequencies considered, the higher the frequency, the higher the wall shear stress was found to be.

Fig. 11 presents the time history of the skin-friction coefficients at several positions on the flat plate for different frequencies. The curves indicate the fluctuations of wall skin-friction coefficient at the specified frequencies at several locations on the flat plate. The fluctuating amplitude of the skin friction at the first calculation station is higher than at the downstream stations where the disturbance has dissipated some of its energy due to mixing. From the results, one can speculate that with a purely sinusoidal travelling-wave external disturbance the wall shear stress would respond sinusoidally and the amplitude of the fluctuations would decrease in the flow direction.

Figs. 12–14 show a comparison of unsteady skin-friction coefficients obtained by calculations, direct measurement using a hot-film probe, and by velocity curve fits as a function of the reduced frequency. Velocity curve fits were made at each station along the flat plate by using the boundary-layer velocity measurements across the boundary layer. The procedure to obtain curve fits through measurement data was to recursively manipulate the data until a best-fit polynomial was obtained. In this case a ninth-order polynomial was found to provide a best fit to most of the data. Equations formulated this way were then evaluated to determine the slope at the surface of the flat plate, and therefore the skin friction.

In the figures, the average value of the unsteady skin-friction coefficient is presented in terms of the reduced frequency ($\varpi = \omega x/U$). For a frequency of 20 Hz, the calculated and experimental results are not in good agreement. The transition-like trend indicated by measurement was not reproduced by curve fitting from velocity data, or by the

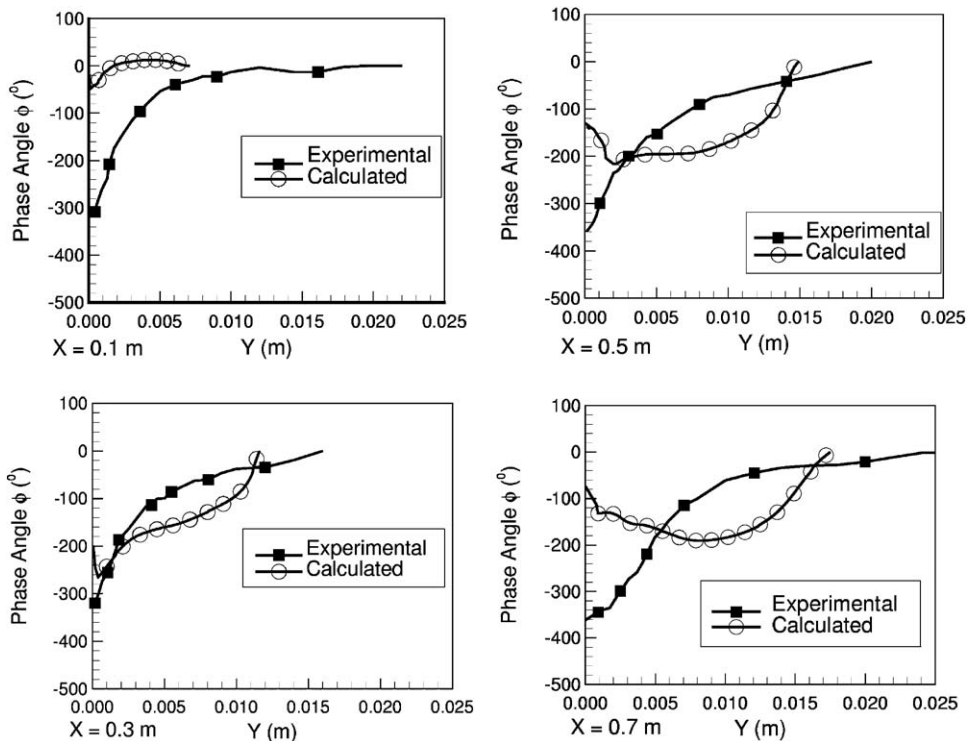


Fig. 8. Comparison of experimental and calculated velocity phase shifts across the boundary layer; $f = 20$ Hz: (a) $X = 0.1$ m, (b) $X = 0.3$ m, (c) $X = 0.5$ m, and (d) $X = 0.7$ m.

calculations. Both calculation methods overestimated the values obtained by measurement. The computational results lie between the curve fit estimate and the measured results. The calculated results, however, tended to converge towards the measured results in the downstream direction.

The discrepancies between the three sets of results appear to narrow down with increasing frequency of free-stream oscillation, as can be seen in Figs. 13 and 14. Although the calculated and velocity curve fit results still overestimate the measured results, the gap closes as the frequency is increased. However, compared to the steady boundary-layer results of Gete (1996), all of the periodically unsteady turbulent boundary layers show significant increases in wall friction. Therefore, in evaluating the wall shear stress for unsteady turbulent boundary layers, one should not rely solely on steady flow results.

Concerning the discrepancy between direct measurement and computational results, one important factor is the assumption of the form of the free-stream fluctuation. Within the computational scheme it was assumed that the free-stream oscillation was sinusoidal. The nonsinusoidal nature of the experimental fluctuations generated by passing rotor wakes was therefore inaccurately modelled by sinusoidal fluctuations in the computational scheme. Moreover, the angular fluctuation in the absolute velocity vector at the rotor exit, that is, before the flow interacts with the boundary layer on the flat plate in the experiments, was not considered in the calculation model. It has also been noted that significant random turbulent fluctuations existed within the wakes of the airfoils, while no turbulent fluctuation was included in the free-stream fluctuating disturbance model used in the calculations. Although it is believed that the major physical phenomena in travelling-wave-type unsteady turbulent boundary layers were predicted by the calculations, more refined modelling of the free-stream periodic fluctuations corresponding to the experimental results is required to close the gap between calculation and experiment.

The greatest differences in skin-friction coefficients are seen between wall shear stress measurement and those obtained from velocity curve fits. One source of error for the velocity curve fit data could be the difficulty of taking measurements of velocities very close to the wall. In fact the velocities were extrapolated to the wall and the wall shear stress was then derived from the velocity gradients. Errors may also be associated with the curve fits to the measured data.

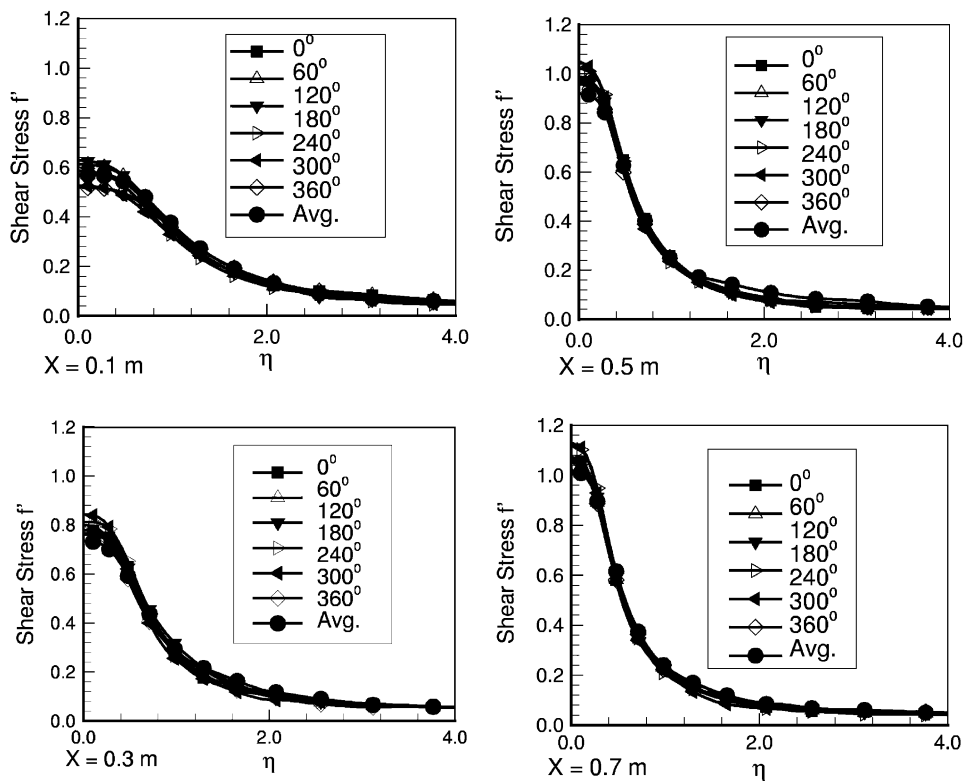


Fig. 9. Calculated shear stress profiles at various phases in a cycle; $f = 30$ Hz: (a) $X = 0.1$ m, (b) $X = 0.3$ m, (c) $X = 0.5$ m, and (d) $X = 0.7$ m.

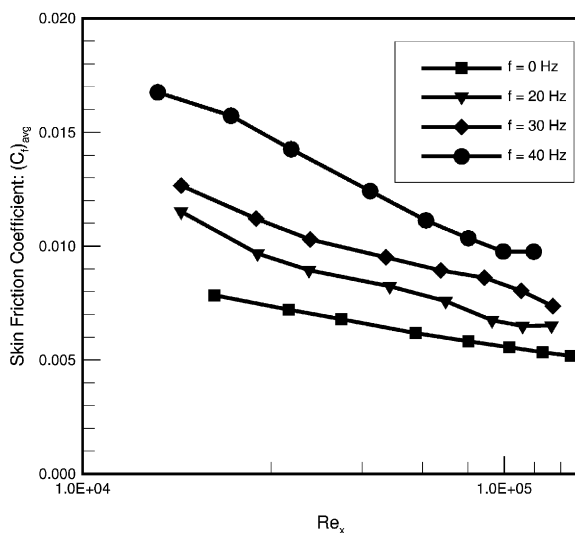


Fig. 10. Computed average skin-friction coefficient at different free-stream disturbance frequencies.

5. Conclusions

The unsteady turbulent boundary-layer calculation procedure, adapted from Cebeci and Carr (1981), and modified to accommodate travelling-wave-type free-stream oscillations following the procedures of Evans (1989), was used for comparison with experimental data. Although the calculations were limited in scope, the results obtained are interesting

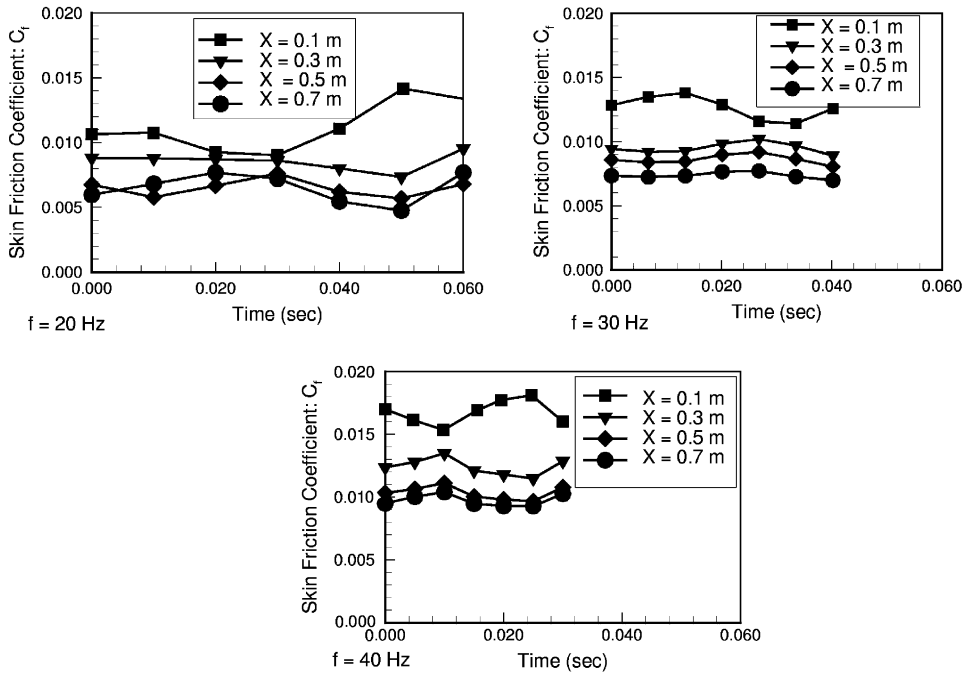


Fig. 11. Time history of skin-friction coefficient along the flat plate.

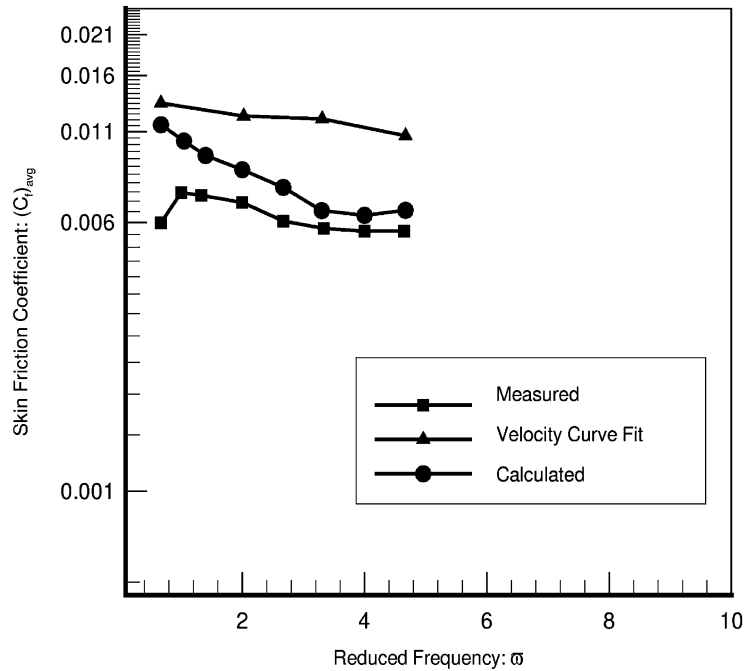


Fig. 12. Comparison of wall skin-friction coefficients obtained by direct measurement, velocity curve fit, and computation; $f = 20$ Hz, $S = 0.1$ m.

and encouraging. The wall shear stress was found to respond strongly to the free-stream disturbance frequency, and to increase with increasing frequency. All results show that high wall shear stress values are observed in unsteady turbulent boundary layers compared to the values in steady flow.

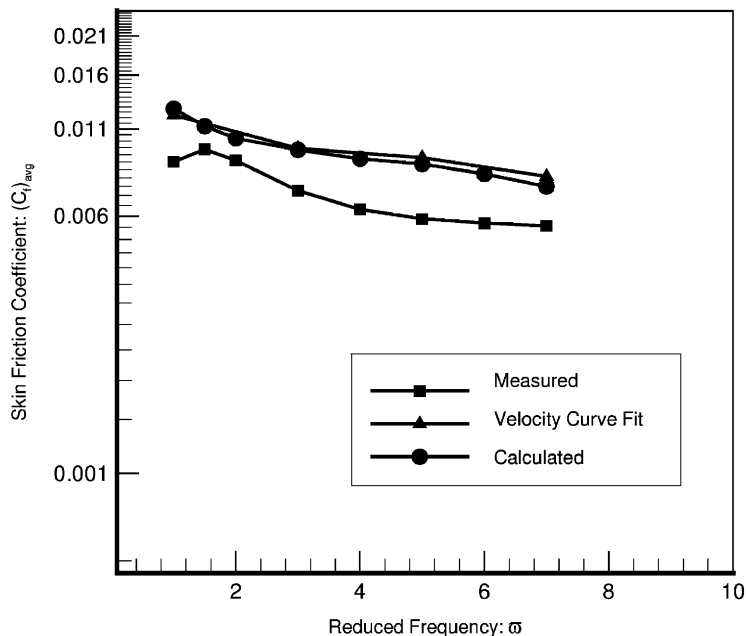


Fig. 13. Comparison of wall skin-friction coefficients obtained by direct measurement, velocity curve fit, and computation; $f = 30$ Hz, $S = 0.1$ m.

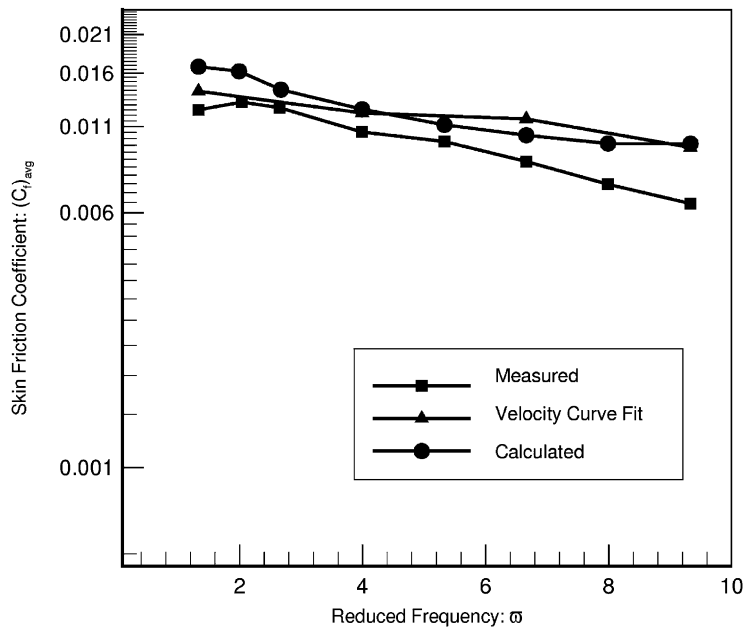


Fig. 14. Comparison of wall skin-friction coefficients obtained by direct measurement, velocity curve fit, and computation; $f = 40$ Hz, $S = 0.1$ m.

Calculations were limited to a free-stream oscillation of about $0.1U_\infty$ and $Re_x = 0.144-1.44 \times 10^5$. The flow was considered turbulent starting from the trip-wire location on the flat plate. The computational scheme is sensitive to time and transverse grid spacing closest to the wall. Calculated average velocity profiles compare reasonably with the experimental velocity profiles with a maximum margin of error of about $\pm 12\%$. Unsteady turbulent velocity profiles

vary significantly within a single period in response to the external fluctuations. The velocity fluctuations are strong in the outer region of the profile. All cases indicate strong fluctuations as a result of nonlinear interactions. This means that caution should be exercised in the use of steady turbulent boundary-layer results in a design process that involves unsteady flows.

The quantitative agreement between calculated and measured phase shifts is poor, although the calculations captured the negative phase shift found in response to travelling-wave perturbations. The negative phase shift of the velocity within the boundary layer for a travelling-wave speed $Q < U_\infty$, was in agreement with earlier experimental studies by Evans and Yip (1988) and Holland and Evans (1999), as well as with the laminar calculations of Evans (1989).

Calculated skin-friction coefficients were found to overpredict experimental results over the range of frequencies tested ($f = 20, 30, 40$ Hz or $\omega = 0.33\text{--}9.33$). However, in all cases the skin friction was found to decrease as the reduced frequency was increased.

Discrepancies between the calculated and experimental results may be attributed to:

- (a) Modelling the wakes of the airfoils by a simple sinusoidal travelling-wave-type free-stream velocity.
- (b) The varying angle of attack of the flow on the flat plate, which was not accounted for in the calculations.
- (c) The random turbulent fluctuations inside the individual wakes which were not considered in the calculations.

In general, for the cases considered, the calculation procedure appears promising. With improved modelling of the travelling-wave-type fluctuations and the angle of attack on the flat plate, the calculation procedure may be further developed to more closely predict unsteady turbulent boundary layers subject to wakes shed from moving blade rows. The computational results show that the mean skin friction in periodically unsteady boundary-layer flow formed as a result of external travelling-wave disturbances should not be estimated with steady flow skin-friction results. Therefore, in approximating skin friction losses in a turbomachine stage flow, there is a clear need to account for losses due to periodic unsteadiness.

References

- Carr, L.W., 1981. A review of unsteady turbulent boundary layer experiments. NASA TM-81297.
- Cebeci, T., Bradshaw, P., 1977. *Momentum Transfer in Boundary Layers*. McGraw-Hill, New York.
- Cebeci, T., Carr, L.W., 1978. A computer program for calculating laminar and turbulent boundary layers for two-dimensional time-dependent flows. NASA TM-78470.
- Cebeci, T., Smith, A.M.O., 1974. *Analysis of Turbulent Boundary Layers*. Academic Press, London, pp. 1–46.
- Evans, R.L. 1988. Unsteady laminar boundary layers subject to standing wave or travelling wave free stream fluctuations. Cambridge University Engineering Department Report, CUED/A-Turbo/TR 124.
- Evans, R.L., 1989. Computation of unsteady laminar boundary layers subject to travelling wave free stream fluctuations. *AIAA Journal* 27, 1644–1646.
- Evans, R.L., Yip, R.S.K., 1988. An experimental investigation of wake–boundary layer interaction. *Journal of Fluids and Structures* 2, 313–322.
- Fletcher, R.H., et al., 1987. Calculation of unsteady turbulent boundary layers. ASME Paper No. 87-GT-53.
- Gete, Z., 1996. A study of unsteady wake–boundary layer interaction in turbomachines. Ph.D. Thesis, The University of British Columbia.
- Gete, Z., Evans, R.L., 2003. An experimental investigation of unsteady turbulent wake–boundary layer interaction. *Journal of Fluids and Structures* 17, 43–55.
- Hill, P.G., Stenning, A.H., 1960. Laminar boundary layers in oscillatory flow. *Journal of Basic Engineering* 82, 593–608.
- Hodson, H.P., 1984a. Boundary layer and loss measurements on the rotor of an axial-flow turbine. *Journal of Eng. for Gas Turbines and Power* 106, 391–399.
- Hodson, H.P., 1984b. Measurements of wake-generated unsteadiness in the rotor passages of axial-flow turbines. ASME Paper No. 84-GT-189.
- Holland, R.M., Evans, R.L., 1999. The effects of periodic wake structures on turbulent boundary layers. *Journal of Fluid and Structures* 10, 269–280.
- Lighthill, M.J., 1954. The response of laminar skin friction and heat transfer to fluctuations in the stream velocity. *Proceedings of the Royal Society of London* 224, 1–23.
- Patel, M.H., 1975. On laminar boundary layers in oscillatory flow. *Proceedings of the Royal Society of London* A347, 99–123.